

Structural Analysis of Amorphous GeO₂ under High Pressure Using Reverse Monte Carlo Simulations

Kenta Matsutani

*Graduate School of Science and Engineering, Yamagata university,
1-4-12, Kojirakawa, Yamagata 990-8560, Japan*

Asumi Yamauchi, Shusuke Kasamatsu, and Takeshi Usuki

*Faculty of Science, Yamagata University,
1-4-12 Kojirakawa, Yamagata 990-8560, Japan*

(Dated: September 10, 2024)

Abstract

The structural properties of amorphous GeO_2 , a prototypical network glass, were investigated under ambient to high pressure using reverse Monte Carlo simulations based on reported structure factors from in situ high-pressure neutron diffraction experiments with isotopic substitution. The results indicate the retention of the topological structure containing predominantly tetrahedral GeO_4 units up to ca. 4 GPa ($\rho/\rho_0 = 1.15$), which is explained by the reduction of cavity volumes. With further application of pressure, an increase in the number of GeO_5 units is first observed, which is then followed more gradually by an increase in the number of GeO_6 units.

I. Introduction

The structural compaction mechanism of vitreous oxides under high pressure has been a topic of high interest in the context of geoscience with the ultimate aim of understanding the nature of Earth's interior [1, 2]. The topic is also of significance from the standpoint of glass theory; characterizing and understanding the nature of pressure-driven transitions in glassy systems is still a difficult and fundamental challenge [3, 4]. A prototypical oxide system under intense study in this regard is GeO_2 . Although its chemical (and to a large extent, structural) analogue SiO_2 is known for more practical applications, GeO_2 is an ideal system for studying structural transition of vitreous oxides because of its higher sensitivity to pressure [5].

At ambient pressure, amorphous GeO_2 is comprised mostly of a network of corner-sharing GeO_4 tetrahedral units. Experimental [6–8] and theoretical [8–12] reports in the literature basically agree that this changes gradually to a network consisting of predominantly octahedral GeO_6 units with increasing pressure. A similar behavior is known for crystalline GeO_2 although the transition occurs much more abruptly [6, 12, 13]. There are some discrepancies among the literature on the details of the transition process, however. For example, Lelong et al. conducted inelastic X-ray scattering (IXS) experiments on compressed amorphous GeO_2 and used crystalline standards to estimate the coordination environment of Ge atoms [7]. They report that five-fold coordinated Ge occurs as a minor component (less than 30%) only in the range of 5 GPa to 8 GPa and acts as a transient species between four- and six-fold coordinated Ge. On the other hand, Wezka et al. have presented a different picture based on a combination of molecular dynamics (MD) simulations employing their

original DIPole-Polarizable Ion Model (DIPPIM) [14, 15] and *in situ* neutron diffraction with isotopic substitution (NDIS) [8, 16]. They first show that DIPPIM reproduces almost perfectly the pressure dependence of the average bond lengths and coordination numbers obtained from NDIS when compared at the same densities (note that MD fails to reproduce the pressure-density relationship, most likely due to the limited timescale in the glass preparation procedure), then go on to interpret local non-average information from MD. The DIPPIM MD results show that the tetrahedral network is sustained up to ~ 4.5 GPa, after which five-fold coordinated Ge starts to increase. Six-fold coordinated Ge also start to appear above ~ 8 GPa, but no suppression of five-fold coordinated Ge appears in contrast to IXS results. It was postulated that the discrepancies stem from using crystalline standards containing trigonal bipyramidal GeO_5 which was found to be rather scarce in DIPPIM results [8]. Various other classical and *ab initio* MD studies can be found in the literature, and the overall behavior is reported to be rather similar to DIPPIM although with some quantitative differences [9–12].

One information that is now lacking is the experimental confirmation of the evolution of the ratio of coordination environments vs. pressure, since neutron diffraction only provides direct information on the *average* coordination and not the local ratios. Also, even though the MD simulation using DIPPIM shows excellent agreement in various average quantities available from NDIS, the agreement of the structure factors is far from perfect, especially at higher pressures [8]. The present study addresses this issue through reverse Monte Carlo (RMC) modeling [17], which attempts to obtain a real-space structure that reproduces the structure factors obtained by the diffraction experiment. A well known issue with RMC modeling based on total structure factors is that they sometimes result in rather “unphysical” results with many homopolar bonds, because partial correlations cannot be deduced from total structure factors. This issue is alleviated to a large extent by using structure factors measured with different isotopic enrichments, i.e., NDIS, which allows for reproduction of the correct partial (Ge–O, Ge–Ge, and O–O) correlations [16]. Here, we perform RMC modeling using NDIS data below 8 GPa and without isotopic substitution up to 17.5 GPa. Coordination numbers and bond angles extracted from the obtained RMC model are compared carefully with previous experimental and computational literature. To complement the analysis, we also performed FPMD simulations of glass formation via a melt-quench approach.

II. Modeling Procedure

RMC modeling of amorphous GeO_2 was conducted using RMC++ code [17]. We employed models containing 3000 atoms (Ge 1000 and O 2000 atoms, respectively) in cubic simulation cells under periodic boundary conditions. The starting atomic configurations corresponding to experimental number density at ambient pressure (0.0629 \AA^{-3} [18]) were generated by a hard-sphere Monte Carlo simulation. Then, RMC modeling was performed based on structure factors $F(Q)$ from high-pressure NDIS [16] from ambient to 8 GPa, and without isotopic substitution at 8.5 GPa to 17.5 GPa ($1.38 < \rho/\rho_0 < 1.64$) [19]. The number density was raised in steps of 0.0629, 0.0727, 0.082, 0.0845, 0.0867, 0.0868, 0.0951, 0.0987, and 0.1031 \AA^{-3} to simulate pressure application. The corresponding experimental pressure values calculated by interpolation of experimental pressure-volume data are 4, 5.9, 6.8, 8.0, 8.5, 11.5, 14.5, 17.5 GPa. The final structure obtained by RMC simulation at each pressure was taken to be the initial structure for the next pressure step. Coordination constraints are used to avoid two- or three-fold coordinated Ge; we judged such coordination environments to be very scarce and ‘unphysical’ based on FPMD results, where no Ge atoms were found with less than four-fold coordination. The cut-off radii used in RMC modeling are tabulated below. (table 1) We detected cavities in the models by determining domains that are farther from any atoms than a cutoff distance of 2.8 \AA using Voronoi construction as implemented in pyMolDyn [20].

FPMD simulations for amorphous GeO_2 were performed with the generalized gradient approximation functional by Perdew-Burke-Ernzerhof (GGA-PBE) [21] implemented in Vienna ab initio Simulation Package (VASP) code [22]. The projector augmented wave method was used to describe electron-ion interactions. The plane wave cutoff energy was set at 289.8 eV, and the self-consistent-field convergence criteria were adopted to be smaller than 10^{-5} eV. Only the Γ point is used in the Brillouin zone sampling. To obtain the glass structure, we first randomly placed 120 atoms (40 Ge atoms and 80 O atoms) in a cubic supercell while keeping all atoms at least 1.8 \AA apart. The cell size was determined so that the number density corresponds to the experimental one for the amorphous phase at ambient pressure. Using the Nosé thermostat, the model was heated up to 3000 K and equilibrated for 40 ps in the liquid state. Subsequently, the model was quenched to 300 K with a rate of 5.0 K/ps, then equilibrated for 40 ps to yield the FPMD-derived structure for amorphous GeO_2 under

TABLE I. The cutoff radius at each pressure controls the closest distance between two atoms in a glass system.

Pressure (GPa)	Ge-Ge (\AA)	Ge-O (\AA)	O-O (\AA)
ambient	2.6	1.6	2.45
4.0	2.6	1.6	2.4
5.9	2.6	1.6	2.3
6.8	2.6	1.6	2.3
8.0	2.6	1.6	2.3
8.5	2.7	1.65	2.2
11.5	2.8	1.7	2.2
14.5	2.625	1.6	2.2
17.5	2.65	1.6	2.2

ambient conditions.

III. Results and Discussion

A. Structure Factors

First, we compare RMC and experimental structure factors in order to confirm our RMC analysis reproduces the structure factor from neutron diffraction with isotope substitution. Figure 1 shows that our RMC model successfully fits all three experimental total structure factors of samples isotopically enriched with ^{70}Ge , ^{73}Ge , and that using natural isotopic abundance of Ge denoted by $^{\text{nat}}\text{Ge}$. Each total structure factor function has the first sharp diffraction peak (FSDP) at 1.5\AA^{-1} , which decreases its magnitude upon compression. On the other hand, the small second peak (principal peak) at ambient pressure increases in intensity with application of pressure; this indicates that pressure application leads to changes in the intermediate-range structure. Thus, we can be fairly certain that our RMC model contains the correct partial correlations.

To further understand the details of structural changes in GeO_2 glass, we examine the partial structure factors shown in figure 2. The pressure-induced changes in partial structure factors show similar features to the total structure factors. At ambient pressure, a FSDP is

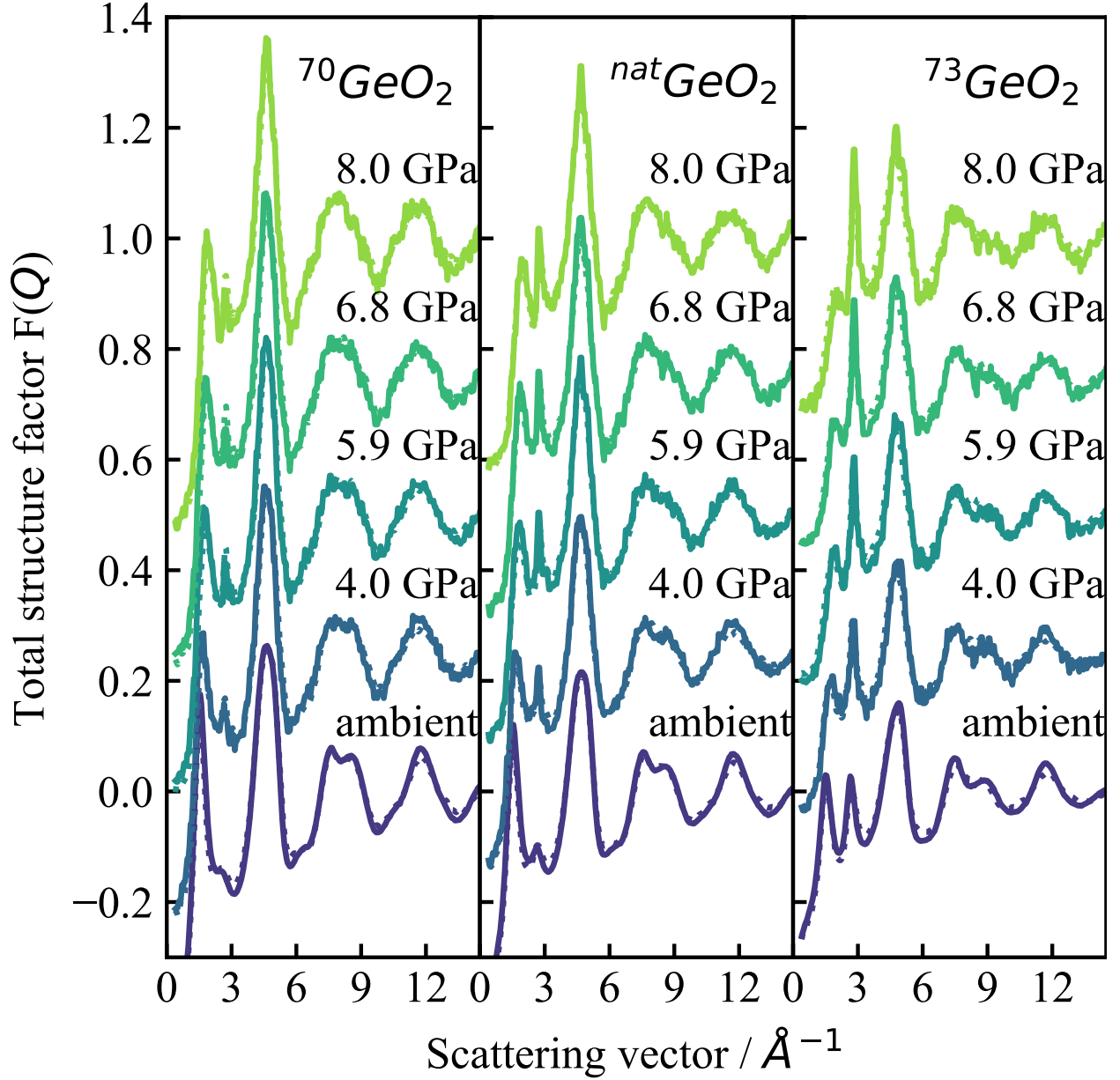


FIG. 1. (Color online) The pressure dependence of total structure factor of amorphous ⁷⁰GeO₂, ^{nat}GeO₂ and ⁷³GeO₂. The solid curves give the experimental data, and the dotted curves represent RMC results.

observed in all partial structure factors. The Ge–Ge and Ge–O FSDPs show similar behavior upon pressure application: the intensities are suppressed and the positions are shifted to higher Q values, finally merging with the principal peak at above 8 GPa. On the other hand, the O–O FSDP is completely suppressed at 4 GPa and above. This correlates well with the annihilation of cavities as will be discussed in Sec. III.D. The principal peak in the O–O

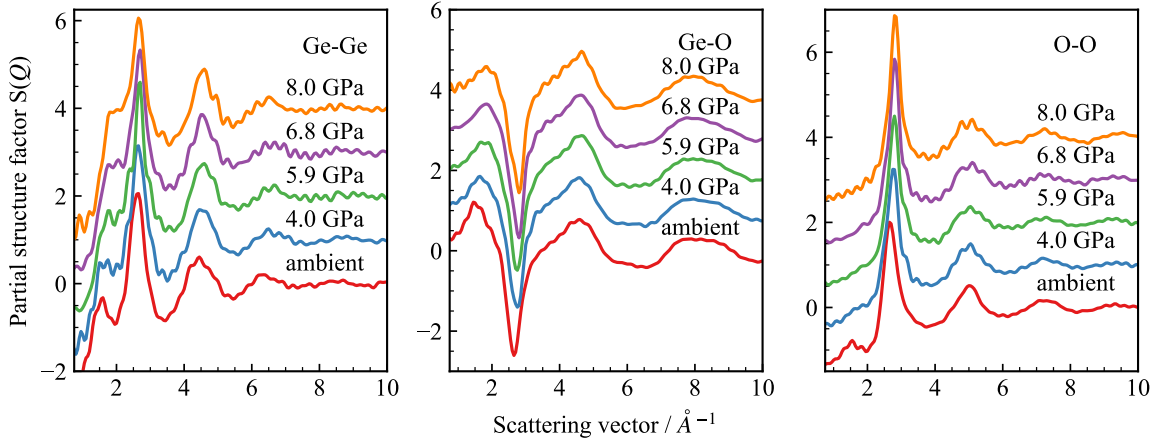


FIG. 2. (Color online) The pressure dependence of partial structure factors for GeO_2 glass. The partial structure factors at ambient pressure, 4.0 GPa, 5.9 GPa, 6.8 GPa, and 8.0 GPa are stacked from bottom to top.

partial structure factor also shifts to higher Q values, but the peak intensity is increased in contrast to the FSDP. This behavior contrasts with that observed for SiO_2 glass [23], as the O-O partial structure factors in SiO_2 glass are almost unchanged under 6 GPa. This is a manifestation of the higher sensitivity of GeO_2 glass structure to pressure compared to SiO_2 .

B. Coordination Number

Coordination number changes around germanium atoms are representative of short-range structural order. The importance of these features have recently been recognized especially in terms of geoscience [23, 24]. Figure 3 shows the fraction of GeO_x ($x = 4, 5, 6$) units calculated from the present RMC results as a function of reduced density and compares them to classical and *ab initio* MD studies and IXS experimental results [7–11]. Our RMC model shows retention of the tetrahedral structure up to $\rho/\rho_0 \sim 1.15$ after which the number of GeO_4 units start to decrease and the number of GeO_5 units start to increase. This signifies the conversion of tetrahedral GeO_4 units to square pyramidal GeO_5 units and is generally in good agreement with the literature. One exception is the MD work by Shanavas *et al.* [9] where no retention is seen and structural transitions occur immediately upon application of pressure. With further compaction, the number of GeO_5 units increase continuously,

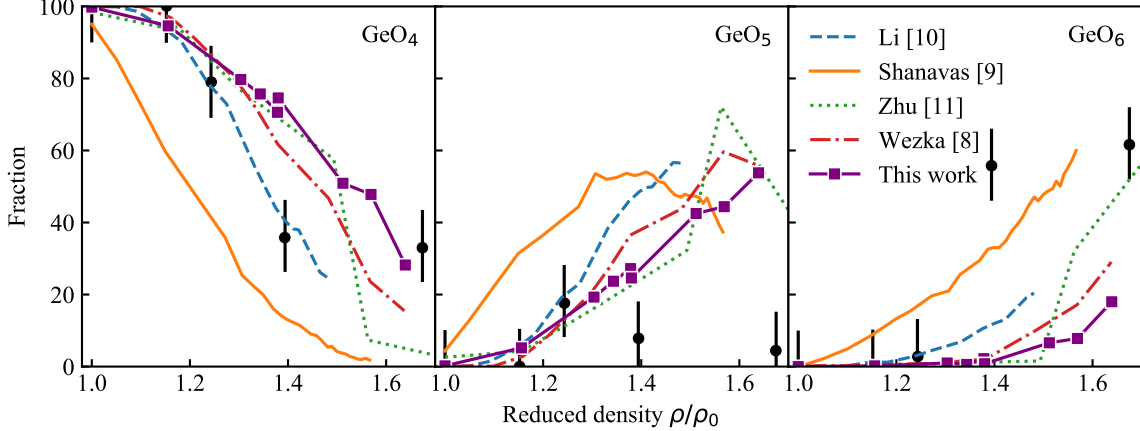


FIG. 3. (Color online) The reduced density dependence of the fraction of GeO_4 (left), GeO_5 (middle) and GeO_6 (right) units in amorphous GeO_2 . The present RMC results (solid curves with squares) are compared to molecular dynamics results in the literature [8–11]. The fractions of GeO_x ($x = 4, 5, 6$) units deduced from IXS experiments [7] are also shown (\bullet with error bars $\pm 10\%$).

reaching 50% at $\rho/\rho_0 = 1.64$. Octahedral GeO_6 units start to emerge more gradually than GeO_5 at about $\rho/\rho_0 = 1.38$, indicating that GeO_5 units act as precursors for conversion to GeO_6 . Again, the general trend is in good agreement with most of the literature. A clear exception is the IXS result [7], which shows emergence of a small amount of GeO_5 units at $\rho/\rho_0 \sim 1.25$ followed by its suppression and a stepwise increase in the number of GeO_6 units. The IXS result is very similar to pressure-induced structural transitions observed in the crystalline phase; thus, Wezka and coworkers [8] suggested that the disagreement stems from using crystalline standards [7], which included trigonal bipyramids as GeO_5 units [25], to analyze IXS results.

C. Bond Angle Distributions

Next, the Ge–O–Ge and O–Ge–O bond angle distributions, which are often used to understand intermediate-range order beyond nearest neighbor atoms, were calculated (Fig. 4). Here, the bond distances of Ge–O were defined by the first minimum in the Ge–O partial pair distribution functions. The O–Ge–O angle distributions are indicative of the Ge-centered structural motifs, while the Ge–O–Ge angle is indicative of the connection between those structural motifs. Much emphasis has been put on obtaining the Ge–O–Ge angles [26, 27]

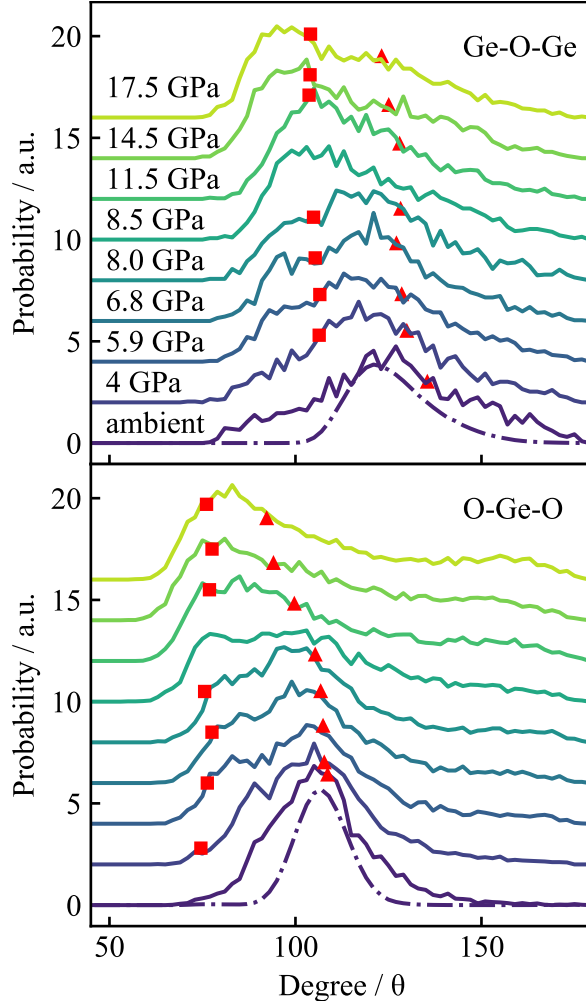


FIG. 4. (Color online) Ge–O–Ge (upper) and O–Ge–O (bottom) bond angle distributions calculated from our RMC models (solid lines) at each pressure, as well as our ambient pressure FPMD result (chained line). The results are compared to bond angles (peaks and shoulders in the bond angle distributions) from classical MD with DIPPIM potentials, where \triangle correspond to GeO_4 motifs and \square correspond to GeO_5 and GeO_6 units. Note the intensity of our FPMD results was divided by 2 for clarity.

because it is a vital parameter in the continuous random network model [28], which is a widely accepted starting point for glass network theory.

Under ambient pressure, the O–Ge–O bond angle distribution has a peak at around 109° , which corresponds to the ideal internal angle in the tetrahedron; this indicates the existence of a dominant tetrahedral structural motif in the amorphous material similar to SiO_2 [26, 29, 30]. Little change is seen in the position of this peak up to 4 GPa, meaning that

amorphous GeO_2 retains most of its tetrahedrally-dominated structure within this pressure range. There is also a shoulder at 120° under ambient condition, which would be a signature of the existence of trigonal bipyramids if there are GeO_5 units. However, analysis of the local coordination, as discussed above, revealed that there are no GeO_5 units at ambient pressure (Fig. 3). Therefore this shoulder originates from distorted GeO_4 units.

Turning our attention to the inter-tetrahedral Ge–O–Ge bond angle, we find that the distribution exhibits a broad peak centered at around 125° , which is about 10° lower than that reported by several works in the literature [8, 16, 26, 27]. The source of this discrepancy will be discussed later. It is also noted that the peak position is much lower than in amorphous SiO_2 whose Si–O–Si peak position is reported to be in the range of 140° – 150° [26, 29, 30]. This peak shifts to a slightly lower angle at 4 GPa, confirming that compaction proceeds via reorganization of corner-sharing tetrahedral GeO_4 units [8].

With further pressure application in the range of $5.9 \text{ GPa} < P < 8.0 \text{ GPa}$, the peak positions shift to lower angles and new peaks around 100° and 90° emerge for Ge–O–Ge and O–Ge–O bond angle distributions, respectively. This indicates that compaction proceeds via corner-sharing tetrahedral units converting to edge-sharing polyhedral units. When $P > 11.5 \text{ GPa}$, the lower side peaks show remarkable increase; clear peaks appear in the O–Ge–O angle distribution around 90° and 170° corresponding to the formation of octahedral GeO_6 units. In the case of amorphous SiO_2 , very little change in the structure has been detected in this pressure range [4, 30].

These results are generally in good agreement with the literature, although quantitative comparison is difficult due to the noisiness in the bond angle distribution (as an example, peaks and shoulders from MD simulation using DIPPIM [8] are compared to the present RMC results in Fig. 4). However, the discrepancy in the Ge–O–Ge angle at ambient pressure is rather clear; the present RMC model shows a Ge–O–Ge (inter-tetrahedral) bond angle centered around 125° , which is about 10° lower than the mean bond angle reported in experimental works [8, 16, 26, 27]. Those works inferred inter-tetrahedral bond angles from simple trigonometric arguments using peak-positions of Ge–O and Ge–Ge pair distribution functions. On the other hand, we used the minimum after the first peak of the Ge–O partial pair distribution function as the cutoff and extracted all Ge–O–Ge within that range from the RMC structure model. Then, the angles of the extracted Ge–O–Ge structures were plotted as distributions. It should be noted that the experimental radial distributions are

also reproduced by the present RMC model, which leads to the same bond angle by using the same simple trigonometric argument. The RMC results are also 10° lower than DIPPIM MD results as well as a report that combined classical MD using an SiO_2 potential with first-principles relaxation [31]; we tentatively suggest that this is because the MD potentials were constructed to reproduce the bond angles reported in experimental works. To confirm the present Ge–O–Ge angle distribution (RMC analysis often result in broader peaks compared to FPMD [32]), we constructed an amorphous GeO_2 model from a melt-quench FPMD simulation and obtained a Ge–O–Ge bond angle peak at the same position as the present RMC result (chained line in Fig. 4). It should also be noted that a previous FPMD work by a different group also reported a peak around 125° .

D. Cavity Analysis

The coordination and bond angle analyses presented above reflect the local structure only up to third nearest neighbor. To complement them with an indicator of the topological network beyond third nearest neighbor, cavity analysis is useful. Cavities are known to influence many materials properties, and its importance has been pointed out particularly for determining SET/RESET behavior in phase change materials [33]. Fig. 5 shows cavity volumes calculated and visualized using pyMolDyn program [20] with a cutoff radius of 2.8 \AA ; these cavities account for 5.7% of the total volume under ambient conditions, while it accounts for only 0.1% of the volume at 4 GPa ($\rho/\rho_0 = 1.15$). This clarifies how compaction proceeds at lower pressures without clear changes in the tetrahedral network structure. The rearrangement of the tetrahedral network, which was indicated by the decrease of the Ge–O–Ge bond angle (Fig. 4), leads to collapsing of cavity volumes. These behaviors can also be correlated with the changes in partial structure factors (Fig. 2). That is, the disappearance of the FSDP in the O–O partial structure factor is seen at the same time as the annihilation of cavities at 4 GPa. Once the cavities are mostly annihilated, the network structure cannot withstand further compaction without changes in the local structural motifs. Kono *et al.* observed pressure-induced behavior of cavities in silica glass by combining molecular dynamics and RMC analysis [34]. Their results are also similar to ours, but the magnitude of changes in the partial structure factors are much smaller due to differences in their pressure sensitivities. It can also be suggested that these cavities may be

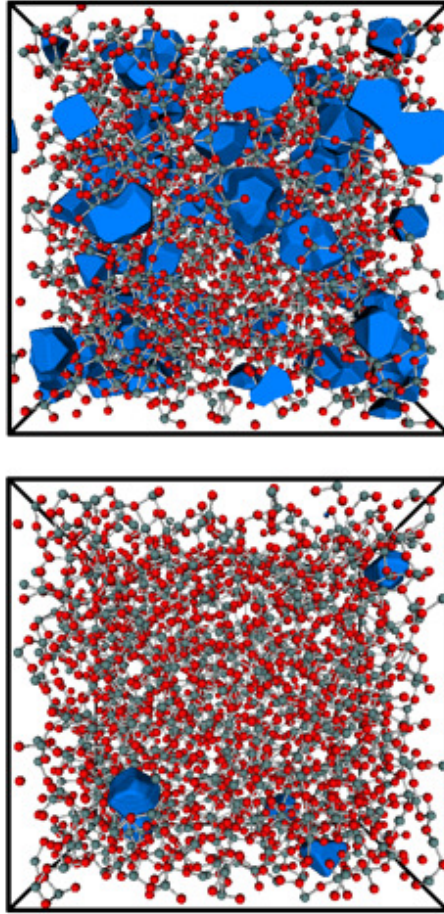


FIG. 5. (Color online) Cavity analysis of the three-dimensional structure obtained by the RMC method. Cavities comprised 5.7% of the total volume under ambient conditions (upper) and 0.1% at 4 GPa (bottom).

the source of the “reversibility window” observed in silica glass [35], as almost no changes in the bond topology are seen below 4 GPa and rebirth of these cavities can be expected upon pressure release.

IV. Conclusion

In this paper, RMC analysis of the structure of amorphous GeO_2 has been performed based on structure factors from NDIS experiments under pressure. The aim was to provide an experiment-based analysis of the local and intermediate-range structure to complement the literature where some discrepancy exists among classical/*ab initio* MD studies and analyses

based on experimental data. The present RMC results are based solely on the experimental structure factors and no assumptions enter the analysis except for minimal coordination constraints noted above. The agreement of RMC results with several MD studies as well as our own FPMD melt-quench simulation thus allows us to confirm the following overall picture of the compaction mechanisms in amorphous GeO₂:

- The amorphous structure under ambient pressure is comprised predominantly of tetrahedral units, and those units are retained up to ~ 4 GPa.
- The compaction below ~ 4 GPa proceeds through collapsing of cavity volumes through buckling of the tetrahedral network structure.
- Further compaction at above ~ 4 GPa after cavities are annihilated require changes in the structural motifs: the tetrahedral units are gradually converted to square pyramidal GeO₅ units at $\rho/\rho_0 > 1.15$, which are, in turn, converted even more gradually to octahedral GeO₆ units at $\rho/\rho_0 > 1.38$.

This work demonstrates the necessity of structure modeling in three-dimensional real space. In this regard, the RMC method combined with NDIS has turned out to be an extremely effective approach.

ACKNOWLEDGMENTS

We gratefully thank Philip Salmon for providing his neutron diffraction data. This research was financially supported by the Japan Society for Promotion of Science (JSPS) KAKENHI Grant Number 16H03903 and 20H02430. Kenta Matsutani and Shusuke Kasamatsu are supported by Japan Science and Technology Agency (JST) FOREST Program (Grant Number JPMJFR2037, Japan).

-
- [1] S. K. Lee, J.-F. Lin, Y. Q. Cai, N. Hiraoka, P. J. Eng, T. Okuchi, H.-k. Mao, Y. Meng, M. Y. Hu, P. Chow, J. Shu, B. Li, H. Fukui, B. H. Lee, H. N. Kim, and C.-S. Yoo: PNAS **105** (2008) 7925.

- [2] S. Petitgirard, C. Sahle, C. Weis, K. Gilmore, G. Spiekermann, J. Tse, M. Wilke, C. Cavallari, V. Cerantola, and C. Sternemann: *Geochem. Persp. Let.* (2019) 32.
- [3] M. C. Wilding, M. Wilson, and P. F. McMillan: *Chemical Society Reviews* **35** (2006) 964.
- [4] Y. Onodera, S. Kohara, P. S. Salmon, A. Hirata, N. Nishiyama, S. Kitani, A. Zeidler, M. Shiga, A. Masuno, H. Inoue, S. Tahara, A. Polidori, H. E. Fischer, T. Mori, S. Kojima, H. Kawaji, A. I. Kolesnikov, M. B. Stone, M. G. Tucker, M. T. McDonnell, A. C. Hannon, Y. Hiraoka, I. Obayashi, T. Nakamura, J. Akola, Y. Fujii, K. Ohara, T. Taniguchi, and O. Sakata: *NPG Asia Materials* **12** (2020) 1. Number: 1 Publisher: Nature Publishing Group.
- [5] M. Micoulaut, L. Cormier, and G. S. Henderson: *Journal of Physics: Condensed Matter* **18** (2006) R753.
- [6] J. P. Itie, A. Polian, G. Calas, J. Petiau, A. Fontaine, and H. Tolentino: *Phys. Rev. Lett.* **63** (1989) 398.
- [7] G. Lelong, L. Cormier, G. Ferlat, V. Giordano, G. S. Henderson, A. Shukla, and G. Calas: *Phys. Rev. B* **85** (2012) 134202.
- [8] K. Wezka, P. S. Salmon, A. Zeidler, D. A. J. Whittaker, J. W. E. Drewitt, S. Klotz, H. E. Fischer, and D. Marrocchelli: *J. Phys.: Condens. Matter* **24** (2012) 502101.
- [9] K. V. Shanavas, N. Garg, and S. M. Sharma: *Phys. Rev. B* **73** (2006) 094120.
- [10] T. Li, S. Huang, and J. Zhu: *Chemical Physics Letters* **471** (2009) 253.
- [11] X. F. Zhu and L. F. Chen: *Physica B: Condensed Matter* **404** (2009) 4178.
- [12] V. V. Brazhkin, A. G. Lyapin, and K. Trachenko: *Phys. Rev. B* **83** (2011) 132103.
- [13] M. Vaccari, G. Aquilanti, S. Pascarelli, and O. Mathon: *J. Phys.: Condens. Matter* **21** (2009) 145403.
- [14] D. Marrocchelli, M. Salanne, P. A. Madden, C. Simon, and P. Turq: *Mol. Phys.* **107** (2009) 443.
- [15] D. Marrocchelli, M. Salanne, and P. A. Madden: *J. Phys.: Condens. Matter* **22** (2010) 152102.
- [16] P. S. Salmon, A. C. Barnes, R. A. Martin, and G. J. Cuello: *J. Phys.: Condens. Matter* **19** (2007) 415110.
- [17] G. Evrard and L. Pusztai: *J. Phys.: Condens. Matter* **17** (2005) S1.
- [18] A. J. Leadbetter and A. C. Wright: *Journal of Non-Crystalline Solids* **7** (1972) 37.
- [19] P. S. Salmon, J. W. E. Drewitt, D. A. J. Whittaker, A. Zeidler, K. Wezka, C. L. Bull, M. G. Tucker, M. C. Wilding, M. Guthrie, and D. Marrocchelli: *J. Phys.: Condens. Matter* **24**

- (2012) 415102.
- [20] I. Heimbach, F. Rhiem, F. Beule, D. Knodt, J. Heinen, and R. O. Jones: *J. Comput. Chem.* **38** (2017) 389.
- [21] J. P. Perdew, K. Burke, and M. Ernzerhof: *Phys. Rev. Lett.* **77** (1996) 3865.
- [22] G. Kresse and J. Furthmüller: *Phys. Rev. B* **54** (1996) 11169.
- [23] M. Guthrie, C. A. Tulk, C. J. Benmore, J. Xu, J. L. Yarger, D. D. Klug, J. S. Tse, H.-k. Mao, and R. J. Hemley: *Phys. Rev. Lett.* **93** (2004) 115502.
- [24] C. Sanloup, J. W. E. Drewitt, Z. Konôpková, P. Dalladay-Simpson, D. M. Morton, N. Rai, W. van Westrenen, and W. Morgenroth: *Nature* **503** (2013) 104.
- [25] D. Cabaret, F. Mauri, and G. S. Henderson: *Phys. Rev. B* **75** (2007) 184205.
- [26] R. Hussin, R. Dupree, and D. Holland: *Journal of Non-Crystalline Solids* **246** (1999) 159.
- [27] J. Neuefeind and K.-D. Liss: *Berichte Bunsenges. Für Phys. Chem.* **100** (1996) 1341.
- [28] W. H. Zachariasen: *J. Am. Chem. Soc.* **54** (1932) 3841.
- [29] A. Pandey, P. Biswas, and D. A. Drabold: *Phys. Rev. B* **92** (2015) 155205.
- [30] M. Micoulaut, Y. Guissani, and B. Guillot: *Phys. Rev. E* **73** (2006) 031504.
- [31] L. Giacomazzi, P. Umari, and A. Pasquarello: *Phys. Rev. Lett.* **95** (2005) 075505.
- [32] J. Akola, S. Kohara, K. Ohara, A. Fujiwara, Y. Watanabe, A. Masuno, T. Usuki, T. Kubo, A. Nakahira, K. Nitta, T. Uruga, J. K. R. Weber, and C. J. Benmore: *PNAS* **110** (2013) 10129.
- [33] J. Akola and R. O. Jones: *Phys. Status Solidi B* **249** (2012) 1851.
- [34] Y. Kono, K. Ohara, N. M. Kondo, H. Yamada, S. Hiroi, F. Noritake, K. Nitta, O. Sekizawa, Y. Higo, Y. Tange, H. Yumoto, T. Koyama, H. Yamazaki, Y. Senba, H. Ohashi, S. Goto, I. Inoue, Y. Hayashi, K. Tamasaku, T. Osaka, J. Yamada, and M. Yabashi: *Nat Commun* **13** (2022) 2292.
- [35] K. Trachenko and M. T. Dove: *Phys. Rev. B* **67** (2003) 212203.